A Hybrid Double Perovskite containing Helium: [He2][CaZr]F6

Anthony J. Lloyd II,[†] Brett R. Hester,[†] Samuel J. Baxter,[†] Shangye Ma,[†] Vitali B. Prakapenka,[‡] Sergey N. Tkachev,[‡] Changyong Park,[%] and Angus P. Wilkinson*,[†],[§]

ABSTRACT: Perovskites are of great technological and geological importance, in large part due to their considerable compositional and structural flexibility. However, the formation of perovskites with neutral species on their A-sites is very unusual. The formation, phase transitions and properties of $[He_2][CaZr]F_6$, which is the first helium containing perovskite to be made, are reported. It is likely that a large family of related materials can also be prepared. On compression in neon, the negative thermal expansion material $CaZrF_6$ amorphizes at ~ 0.5 GPa. However, on compression in helium at room temperature, gas is inserted into the structure to form a perovskite with helium on the A-site. This suppresses the amorphization until > 3 GPa. Volume versus pressure and Raman measurements suggest that filling of the A-site, to give $[He_2][CaZr]F_6$, is complete at > 1 GPa. The presence of helium on the A-site in this perovskite leads to a reduction in the magnitude of negative thermal expansion when compared to the parent phase $CaZrF_6$, likely due to steric impediment of the transverse vibrational motion of fluoride. Helium also leads to considerable stiffening of the structure. At room temperature and ~ 2.5 GPa, the helium containing hybrid perovskite has a bulk modulus of ~ 47 GPa, whereas $CaZrF_6$ has a bulk modulus of ~ 40 GPa at ambient. Cubic perovskite $[He_2][CaZr]F_6$ undergoes a structural phase transition at 15 K on compression, which may involve a cooperative tilting of framework octahedra to give a lower-symmetry phase, which is tentatively assigned as tetragonal.

INTRODUCTION

Since the report of Xe[PtF₆] in 1962 by Barlett, noble gas chemistry has undergone considerable development. The oxide and fluoride chemistry of xenon is now quite extensive, and examples of molecular compounds containing xenon-xenon bonds,² xenon gold bonds,³ and xenon carbon bonds are known. Oxides with perovskite and layered perovskite structures with xenon on the B-sites have been prepared.^{4,5} The existence of intermetallic phases, containing xenon serving as an electron donor, has been proposed under conditions similar to those found in the Earth's core, based on structure searching and first principles calculations, and experimentally established. However, the chemistry of the lightest noble gas, helium, is far less developed than that of its heavier group members. The application of high pressure is known to modify the bonding in materials and open up new chemical possibilities,8 and computation and experiment at high pressures, is now revealing a varied and fascinating solid state chemistry for helium.

The formation of helium hydrates at modest (< 1 GPa) pressure, by insertion into the ice-II structure, was first established in $1988^{9,10}$ and shortly afterwards helium was shown to form van der Waals solid compounds, such as $He(N_2)_{11}^{11}$ and $Ne(He)_2^{12}$ at moderate (~ 10 GPa) pressures. Helium is widely used as a pressure transmitting

medium in diamond anvil cell experiments, even though it is not always benign. It has been observed to penetrate into silica glass at high pressures and change its properties. 13,14 It has also been shown to be included at high pressure into a variety of crystalline compounds such as cristobalite, 15 arsenolite, 16,17 and the silica clathrate melanophlogite, 18 leading to changes in phase behavior and other properties. The diversity of bonding in helium compounds was advanced considerably with the theoretical prediction and experimental verification that Na₂He is stable at high pressure (> 113 GPa). 19,20 This compound is a fluorite structure electride, where helium serves as a spacer between the sodium cations and pockets containing electrons. There have been predictions that helium can serve as a template for the formation of a very high energy density polymeric nitrogen phase, HeN₄, at moderate pressure (~8.5 GPa)²¹ and that it can react with a wide range of ionic compounds above 30 GPa, to form compounds such as CaF₂He, where helium modifies the interactions of the cation and anions.²² Interestingly, the formation of helium and neon containing compounds by reaction with alkali oxides and sulfides has been predicted to occur a modest pressures, with NeCs₂S potentially stable at ambient conditions. ²³ FeO₂He has been proposed as a possible reservoir for helium under deep Earth conditions (> 125 GPa)²⁴ and the formation of FeHe has been predicted²⁵ under conditions (~4 TPa) similar to those of the core man-

[†] School of Chemistry and Biochemistry, Georgia Institute of Technology, Atlanta, GA 30332-0400, United States

[§] School of Materials Science and Engineering, Georgia Institute of Technology, Atlanta, GA 30332-0245, United States

[‡]Center for Advanced Radiation Sources, University of Chicago, Chicago, Illinois 60637, United States

[%] HPCAT, X-ray Science Division, Argonne National Laboratory, Argonne, Illinois 60439, Unite States

tle boundary for Jupiter. Recently, several groups have computationally investigated the insertion of helium into H_2O and NH_3 at high pressure. The driving force for the formation of new phases includes a component from the modification of electrostatic interactions on helium insertion, and superionicity involving the diffusion of protons and/or helium has been predicted for some helium water and helium ammonia phases.

Much of the recent work on novel solid helium compounds has focused on moderate to very high formation pressures (10 GPa – 4 TPa). However, it has recently been shown that helium will insert into the ReO₃-type material CaZrF₆ at low pressures, resulting in the formation of a defect perovskite $[He_{2-x}\square_x][CaZr]F_{6}$, which could be recovered to ambient pressure at low temperature. This is the first example of a perovskite with helium as a structural component and, as there are many known ReO₃-type fluorides, ^{30,31} several of which show large isotropic negative thermal expansion (NTE), ^{32,34} there is considerable scope for developing a new family of hybrid gas containing perovskites and exploring their properties. As a high volumetric density of gas can be trapped in these materials and recovered to ambient pressure, application in gas storage and separation may be possible.

The current work advances the previous study of helium insertion into $CaZrF_6$, which was limited to a maximum pressure of 0.5 GPa leading to $x \sim 1.0$ for $[He_{2-x}\Box_x][CaZr]F_6$. High-pressure synchrotron diffraction experiments, using diamond anvil cells (DACs) along with helium and neon as pressure media, were performed to estimate the pressure required for formation of the stoichiometric perovskite $[He_2][CaZr]F_6$ and examine the high-pressure behavior of this material. These experiments were complemented by a Raman study. A diffraction experiment in a DAC at low temperature was also performed to explore the thermal expansion and phase transitions of $[He_2][CaZr]F_6$.

2. EXPERIMENTAL

2.1. Synthesis of CaZrF₆

 CaF_2 (99.5%, Sigma Aldrich) and ZrF_4 (99.9%, STREM) were used to prepare $CaZrF_6$ via solid state reaction using a procedure adapted from Hancock el al.³³ A 1:1 molar ratio of starting materials was thoroughly ground together under dry nitrogen. The reactant mixture was pressed into a pellet and loaded into a nickel tube. The tube was sealed by arc welding under argon and then sealed inside an evacuated fused silica ampoule. The reaction mixture was heated to 750 °C, held at 750 °C for 48 h, and then cooled to room temperature.

2.2. High-Pressure Ambient Temperature Diffraction Measurements

High-pressure powder X-ray diffraction data were collected using GSECARS beamline 13-BMD at the Advanced Photon Source, Argonne National Laboratory. Diffraction data were recorded on a Perkin-Elmer amorphous silicon 2D detector using a wavelength of 0.3344 Å. The detector geometry was calibrated using a NIST LaB6 standard. A defocused beam (~100 x 100 μm) was used in order minimize difficulties with sampling statistics, as CaZrF6 disorders on heavy grinding. In each experiment, the samples were compressed in

BX-90 diamond anvil cells equipped with 800 μm culet diamonds and stainless-steel gaskets (400 μm holes). Helium and neon, loaded using the high-pressure gas loading system at GSECARS, were used as pressure transmitting media. The known equation of state and the measured lattice constants of CaF2 or NaCl were used to determine the pressure. 36,37

2.3. Low-Temperature, High-Pressure Diffraction Measurements

Low-temperature diffraction data were acquired using beam line 16-BMD at Argonne National Laboratory's Advanced Photon Source (APS). The sample was mixed and ground in a \sim 4:1 volume-to-volume ratio with sodium chloride, for use as a pressure calibrant, prior to loading into a symmetric DAC equipped with 600 µm culet diamonds. Ruby spheres were included in the cell for pressure estimation. The DAC was initially sealed with helium (~0.25 GPa) as a medium using the high-pressure gas loading system at GSECARS.³⁵ The cell was mounted on the cold finger of an in vacuum helium flow cryostat and equipped with compression and decompression diaphragms for pressure control. Data were taken at a wavelength of 0.49594 Å (25 keV), using a defocused beam to help with sampling statistics (~50 µm FWHM), and recorded on a MAR345 image plate detector. The reported pressures were estimated from the unit cell volume of the NaCl using a third-order Birch-Murnaghan equation of state. Values of $V_0(T)$ and $K_0(T)$ for the EoS (see Table S3) were estimated from thermal expansion data in Touloukian³⁸ and a polynomial expression for the temperature dependence of the compressibility reported by Wang and Reeber.³⁹ K₀' was assumed to be 5 at all temperatures.

Data were recorded at 300 K as the pressure was increased in steps to \sim 2.3 GPa. The sample was then cooled to 200 K, while still under pressure. Data were then taken above \sim 1.9 GPa at 200 K. The DAC was warmed back to 300 K, and adjusted, prior to recooling to 200 K at \sim 1.5 GPa. After collecting further data between 1.3 and 1.5 GPa at 200 K, the sample was cooled to 100 K at \sim 1.5 GPa. After collecting data at 100 K, the sample was further cooled to 15 K while under pressure (\sim 1.5 GPa). Data were then collected on compression at 15 K. The pressures used for the measurements are given in the SI.

2.4. Reduction, Le Bail, and Rietveld Analyses of the Powder Diffraction Data

For the powder diffraction data collected on 13-BM, the 2D data were integrated and the resulting 1D data background subtracted using DIOPTAS. The 2D data collected on 16-BM were integrated using GSAS-II. Le Bail and Rietveld refinements were performed using the General Structure Analysis System (GSAS), coupled with EXPGUI, or GSAS-II, to determine unit cell volume as a function of pressure. A cation-ordered cubic ReO3-type model ($Fm\overline{3}m$) was used in all the Le Bail and Rietveld analyses of the cubic phase , while the I4/m tetragonal space group was used for the low-temperature, high-pressure phase observed at 15 K.

2.5 High Pressure Raman Measurements

Raman spectra were recorded using the optical spectroscopy system for diamond anvil cell studies at GSECARS,⁴⁴ Advanced Photon Source, Argonne National Laboratory, using an excitation wavelength of 532 nm. The sample was ground and loaded into BX-90 DACs along with ruby spheres for pressure calibration. One DAC was gas loaded with neon, and the other with helium, using the GSECARS gas loading system for DACs.³⁵ The spectra were fitted using the commercial software package Origin 9.7. A quadratic function was used for the background. Typically, three independent Lorentzians were used to fit the region around 235 cm⁻¹. Some of the spectra suffered from considerable peak overlap in this region.

3. RESULTS AND DISCUSSION

3.1 Response of CaZrF₆ to Compression in Helium and Neon at Ambient Temperature

Two independent, high-pressure diffraction experiments using CaZrF6 in a helium pressure medium were conducted at 13-BMD. In one case CaF2 was used as an internal pressure standard and, in the other, NaCl was used. Rietveld fits to the data recorded at the starting pressures (0.28 GPa, 0.21 GPa) for these measurements are shown in the supplementary material (Fig. S1 and Fig. S2). The overall fit quality is quite good. However, in both cases, there are two impurity peaks at ~ 1.2 and $1.7\ \mbox{Å}^{-1}$. These peaks were not present in the diffraction pattern of the sample prior to grinding the material for loading into the DACs, but we have previously observed them for samples of CaZrF6 and related materials that have been heavily ground suggesting that this phase arises from the stresses generated during grinding. As the peaks from the impurity do not overlap significantly with those from cubic CaZrF6, they should not adversely affect the lattice constants estimated for CaZrF6.

High-Q data from the set of measurements in helium with NaCl as the pressure standard are shown in Figure 1a. Interestingly, the peaks from cubic CaZrF₆ visibly shift to lower Q between ~ 0.3 and 0.7 GPa, indicating an increase in unit cell volume due to the insertion of helium into the empty "A-site" of ReO3-type structure. This is in agreement with our previously reported (0 - 0.5 GPa) neutron diffraction study, but shows that helium continues to be inserted up until at least ~0.7 GPa.²⁹ Using X-ray diffraction data, it is not possible to determine the site occupancy for helium and directly demonstrate the helium content of the high pressure perovskite phase. However, based on the changes in unit cell volume versus pressure (Figure 2) and the changes in the observed pressure dependence of the vibrational modes noted in our Raman experiment (see section 3.2), complete occupancy of the A-site with helium at ~1.0 GPa is likely. Diffraction peaks from the helium-containing perovskite $[He_2][CaZr]F_6$ persists up to > 3 GPa where a gradual amorphization occurs. It is unclear if the amorphization is associated with the extrusion of helium from the structure, or if some helium is trapped in the amorphous product. No sample peaks remain above ~ 6 GPa. This behavior contrasts with that seen on compression in neon (Figure 1b). The CaZrF₆ begins to disorder at pressures above ~0.5 GPa, which is consistent with the previously reported behavior in silicone oil, 33 indicating that, unlike helium, neon can't be inserted into CaZrF₆ at room temperature.

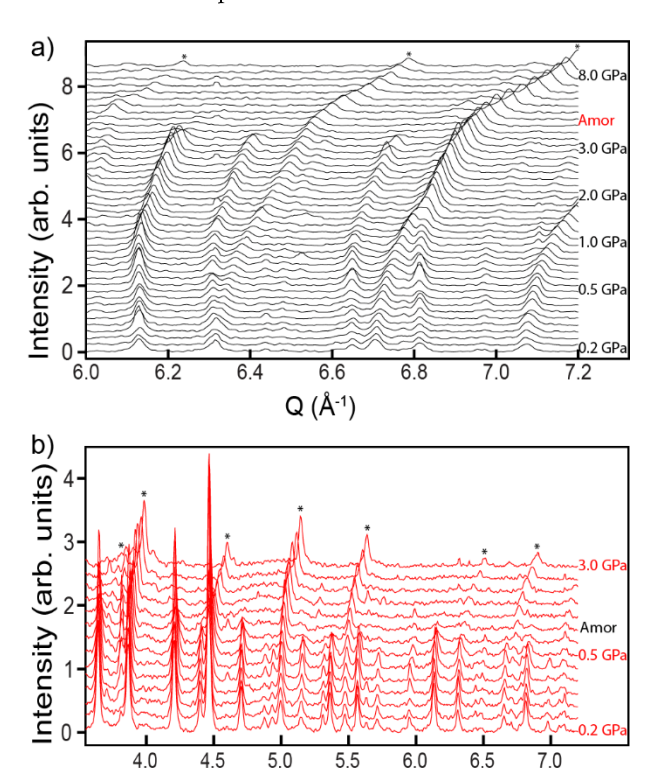


Figure 1. High-pressure X-ray diffraction data for CaZrF₆ in a) helium and b) neon. Peaks from the NaCl pressure standard are marked *.

Q (Å-1)

Unit cell volume versus pressure in helium, obtained using Le Bail fits, is shown in Figure 2. The two sets of experiments with different internal pressure standards are in very good agreement. The inset in Figure 2 clearly shows that on initial compression the unit cell volume decreases, but between ~0.35 and 0.7 GPa it increases, which is attributable to the insertion of helium into the structure. The inserted helium stabilizes the cubic perovskite up to ~ 3.5 GPa. There is an approximately linear variation of unit cell volume with pressure between ~ 1 and 3.5 GPa, although the slight curvature indicates that, unlike most solids, the material's bulk modulus decreases on compression. A linear fit to lnV vs P over the range 1.5 - 3.6 GPa gave estimated average bulk moduli of 48.8(1) and 45.5(8) GPa (see Fig. S3 in the SI) for the experiments using CaF2 and NaCl as internal pressure calibrants, respectively, and a similar fit over the pressure range 1.2 - 1.9 GPa gave estimated bulk moduli of 57(2) and 62(2)GPa. These values are significantly larger than those for CaZrF₆ with no helium inside (~40 GPa at < 0.31 GPa),³³ indicating that helium on the perovskite A-site stiffens the structure, presumably by steric interactions with the fluoride, which impede their transverse vibrational motion as the material is compressed. The observed pressureinduced softening, a decrease in bulk modulus on compression, could be a consequence of lattice dynamics, as NTE frameworks are well known to display this phenomenon. 45,46 However, it could also be associated with the extrusion of helium from the structure prior to its pressure-induced amorphization.

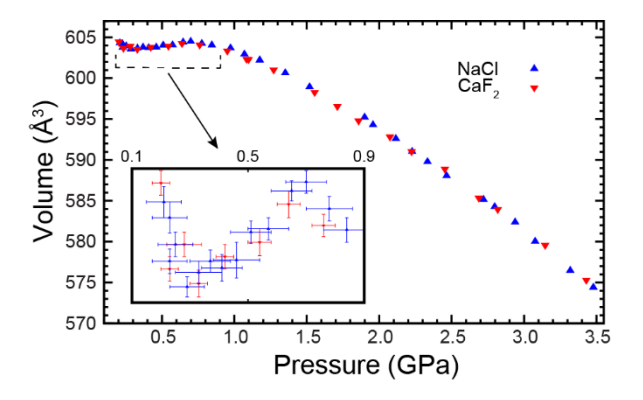


Figure 2. A comparison of unit cell volume for $CaZrF_6$ versus pressure in helium for experiments with NaCl and CaF_2 as pressure calibrants. Inset shows details of the low-pressure behavior. The error bars are one estimated standard deviation, as obtained from the Rietveld derived unit cell volume uncertainties.

3.2 Raman Spectra on Compression

The ambient pressure Raman spectrum of CaZrF₆ has major peaks at 235 and 635 cm⁻¹, and a less prominent broad feature at ~600 cm⁻¹ 1 . These peaks have previously been assigned as F_{2g} , A_{g} and E_{g} modes, respectively, in an elevated temperature Raman study of CaZrF₆.⁴⁷ On the basis of a DFT calculation, the F_{2g} mode was determined to involve the displacement of fluoride transverse to the Ca - Zr vectors, whereas the A_g mode was associated with a breathing type motion.⁴⁷ Figure 3 shows the evolution of the spectra on compression in neon (Fig. 3a) and helium (Fig. 3b). On compression above ~0.55 GPa in neon, the peaks associated with the F_{2g} and A_g modes largely disappear, consistent with the loss of long range order seen in the diffraction measurements (Figure 1b). The peaks that remain and/or seem to grow in on compression at close to 200 cm⁻¹ (Figure 3) may arise from the product formed on disordering, or possibly a phase that formed on originally grinding the sample. If they are growing in as a consequence of disordering, the data in Figure 3b would suggest that some disordering took place for the sample in helium at 1.4 GPa or less. The behavior on compression in helium is distinct from that in neon. The signal associated with the F_{2g} and A_{g} modes persists until over 3 GPa. This is again consistent with the corresponding diffraction data, which show the perovskite phase persisting to ~ 3.5 GPa.

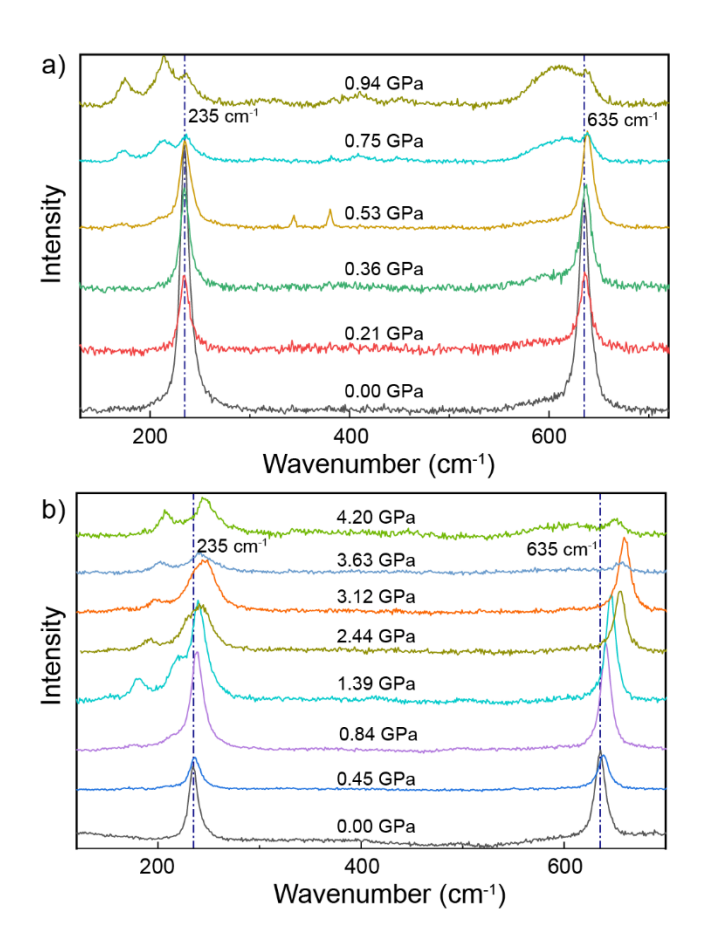


Figure 3. Selected Raman spectra on compression of $CaZrF_6$ in a) neon and b) helium. Their background has been subtracted.

The peak shifts on compression for the sample in helium are distinct from those seen in neon (Figure 4). The F_{2g} mode frequency is essentially invariant with pressure in neon, consistent with the prior report that the Grüneissen parameter for this mode is almost zero.⁴⁷ However, in helium this mode stiffens on compression, presumably as a consequence of gas being inserted into the structure and impeding the transverse vibrational motion of fluoride. The stiffening on compression appears to vary with pressure, consistent with filling the vacant A-sites in the ReO₃- structure at low pressure (< 1 GPa) followed by compression of a completely filled helium perovskite at higher pressures. The FWHM of the peak assigned to the F_{2g} mode increased almost linearly on compression in helium, from ~ 10 cm⁻¹ at 0 GPa to 21 cm⁻¹ at ~ 2 GPa, but no change in peak width with pressure was observed for the A_g mode at < 3 GPa. The A_g mode stiffens on compression in both neon ($\sim 4 \text{ cm}^{-1}/\text{GPa}$, over 0 - 0.75 GPa) and helium, but to a greater extent in helium (~8 cm⁻¹/GPa, over 0 – 3 GPa), consistent with the formation of a helium containing perovskite and its assignment as a breathing mode.

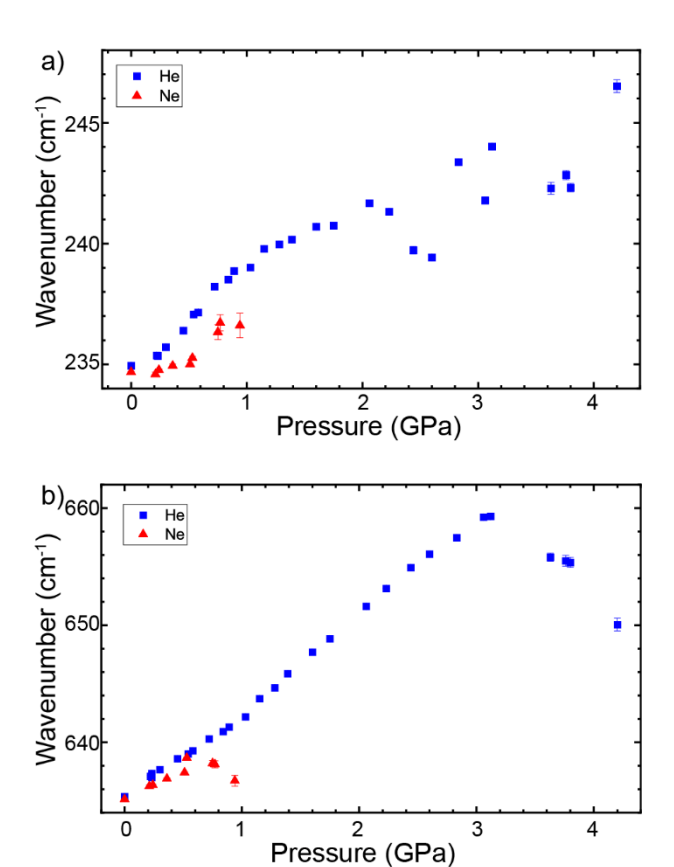


Figure 4. Raman peak positons for the a) F_{2g} and b) A_g zone center modes as a function of pressure for $CaZrF_6$ in neon and helium. The error bars are one standard error, as obtained from least squares fitting of the spectra. In cases where no error bar is visible, the standard error is less than the symbol size.

3.3 Low-Temperature Behavior of [He₂][CaZr]F₆

Perovskites are well known to display a rich array of phase transitions in response to changes in thermodynamic conditions, many of which involve the cooperative tilting of octahedra. A low-temperature, high-pressure diffraction study of $CaZrF_6$ in helium was conducted to study the thermal expansion, elastic stiffness and phase behavior of $[He_2][CaZr]F_6$ at low temperature. All the cooling steps were done at sufficiently high pressure (>1.5 GPa) that essentially complete occupancy of the perovskite A-site by helium is anticipated based on the data shown in Figures 2 and 4. However, complete occupancy could not be directly verified.

Unit cell volumes, obtained by Rietveld analyses of the data, are shown in Figure 5. The overall behavior on compression at 300 K is the same as that observed in the earlier ambient temperature experiments, with a local maximum in the volume at ~0.8 GPa. However, the volume at the local maximum is not as high as that seen in the earlier measurements. The reason for this difference is not clear, although the $CaZrF_6$ sample and the extent of grinding were different for the two experiments. On cooling successively to 200, 100, and 15 K, the volume per formula unit of the material increased, for pressures < 1.6 GPa, indicating that the insertion of helium into the ReO_3 -structure to create a perovskite did not completely suppress its negative thermal expansion. The general behavior of volume versus

pressure at 100 K diverges from that seen at 300 K below \sim 1.2 GPa, suggesting that at 100 K helium is trapped in the framework structure as the pressure is reduced. This is consistent with previous neutron diffraction and direct gas uptake and release measurements performed at < 0.5 GPa.²⁹

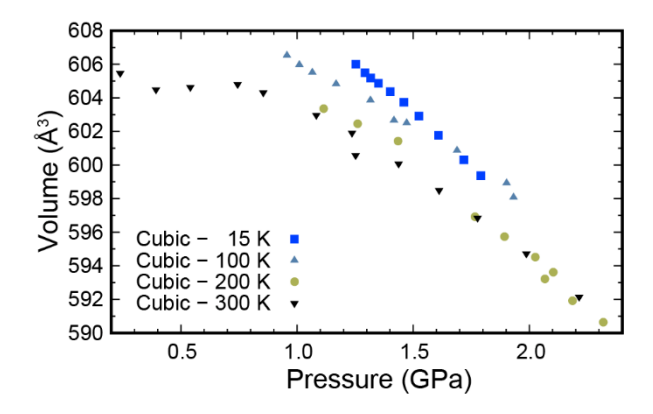


Figure 5. Unit cell volume for cubic $CaZrF_6$ in helium versus pressure at different temperatures. The Rietveld estimated errors in the unit cell volume are smaller than the symbol size.

The sample's bulk moduli, estimated by fitting a straight line to $\ln(V)$ versus P over the pressure range 1.2-1.9 GPa, were 70(10), 53(5) and 76(8) GPa for 300, 200, and 100 K respectively, suggesting no statistically significant change in stiffness on cooling. The same method for estimating the bulk modulus gave values of 57(2) and 62(2) GPa from the room temperature data discussed in section 3.1.

Volume coefficients of thermal expansion (CTE) were estimated at $\sim\!1.2$ and 1.4 GPa from the data shown in Figure 5. In both cases the average CTE over the temperature range 300 to 15 K was close to $\sim\!24\,\mathrm{ppmK^{\text{-}1}}$. Negative thermal expansion in framework materials such as CaZrF6 originates from low-frequency vibrational modes that display pressure-induced softening; in other words, they have negative mode Grüneisen parameters. 45 The parent material, CaZrF6, shows a volume CTE of -45 ppmK-1 over the same temperature range at ambient pressure. The apparent large reduction in the NTE, on inclusion of helium, is presumably because helium serves to sterically impede vibrational motions that are important to the framework's NTE.

Compression at 15 K led to peak broadening and the appearance of shoulders for some peaks in the diffraction data (Figure 6), likely indicating a phase transition. Based on the observed peak broadening, the onset of this transition appears to be at ~ 1.8 GPa. The splittings at the highest pressure (~2.9 GPa) were compared with those predicted, for symmetry lowering octahedral tilting transitions in cation-ordered double perovskites, by Howard et al.⁴⁹ The peak splitting pattern is not consistent with the $Fm\overline{3}m$ to $R\overline{3}$ transition that is often seen on cooling or compressing cation-ordered double ReO₃-type fluorides.^{34,50,51} While the symmetry of the high-pressure phase cannot be assigned definitively based on the available data, due to its modest quality (see Figure S4), the peak broadening is consistent with tetragonal or perhaps lower symmetry. Given the limited quality of the data, we did not pursue an analysis with symmetry lower than tetragonal. Howard et al.⁴⁹ proposed two possible subgroups for

a simple second-order transition to a tetragonal phase, 14/m ($a^0a^0c^-$) and P4/mnc ($a^0a^0c^+$) (see Fig 6b). Fits to the data using the space group I4/m were used to estimate lattice constants, volume per formula unit and a bulk modulus for the high-pressure phase (see Fig. 6c). Surprisingly, c/a is estimated to be less than sqrt(2), which is not what is expected for a transition involving the tilting of undistorted octahedral. The bulk modulus, based on the tetragonal model, is estimated to be ~ 33 GPa, which is lower than that of its cubic parent.

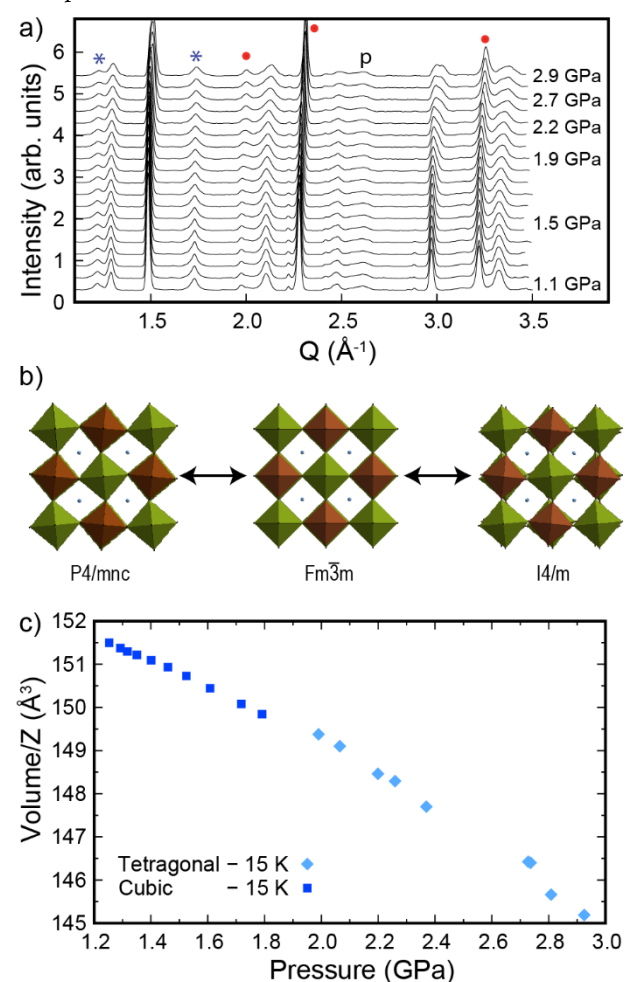


Figure 6. a) Diffraction data on compression at 15 K. Bragg peaks from the sample, between 2.9 and 3.5 Å $^{-1}$, clearly broaden and split on compression, indicating a structural phase transition in He₂CaZrF₆. Blue asterisks - Bragg peaks from a phase formed during the grinding of cubic CaZrF₆. Red circles - Bragg peaks from the NaCl pressure calibrant. p – parasitic scattering from the cell/cryostat. b) Possible tetragonal structures generated by octahedral tilting on compression. c) Volume per formula unit versus pressure at 15 K.

4. CONCLUSIONS

Helium can be inserted at 300 K into the cation-ordered ReO₃-type fluoride CaZrF₆ to form a perovskite with helium on the A-site. The change in unit cell volume versus pressure and the change in Raman mode frequency on compression both suggest that this process is complete by $\sim 1~{\rm GPa}.$ The insertion of helium stabilizes the ReO₃-

type framework against amorphization on compression, and the perovskite persists until > 3 GPa. It is unclear if the amorphous product formed at higher pressures contains helium. The perovskite $[He_2][CaZr]F_6$ displays NTE, although its magnitude is much lower than that of the parent CaZrF_6 phase, which is presumably due to changes in lattice dynamics associated with helium insertion. Remarkably, the interaction with helium is not enough to completely suppress NTE. Raman data directly show that helium insertion leads to an enhanced stiffening of the Raman active modes on compression. $[He_2][CaZr]F_6$ has a greater bulk modulus than cubic CaZrF_6. This change in properties is consistent with helium on the A-site sterically interfering with transverse vibrational motion of the fluoride. At 15 K, a phase transition was observed on compression above ~1.8 GPa, that is tentatively assigned to a cooperative tilting of the framework octahedra leading to a tetragonal phase.

ASSOCIATED CONTENT

Supporting Information. Synthetic details, example Rietveld fits, bulk modulus estimates, lattice constants versus temperature and pressure. This material is available free of charge via the Internet at http://pubs.acs.org.

AUTHOR INFORMATION

Corresponding Author

* angus.wilkinson@chemistry.gatech.edu

ORCID

Angus P. Wilkinson: 0000-0003-2904-400X

ACKNOWLEDGEMENT

We are grateful for experimental assistance from the staff of beamlines 13-BMD and 16-BMD at the Advanced Photon Source. The work at Georgia Tech was partially financially supported under NSF DMR-1607316 and NSF DMR-2002739. Part of this work was performed at GeoSoilEnviro-CARS (The University of Chicago, Sector 13), Advanced Photon Source (APS), Argonne National Laboratory. GeoSoilEnviroCARS is supported by the National Science Foundation – Earth Sciences (EAR – 1634415) and Department of Energy- GeoSciences (DE-FG02-94ER14466). Part of this work was performed at HPCAT (Sector 16), Advanced Source (APS), Argonne National Laboratory. HPCAT operations are supported by DOE-NNSA's Office of Experimental Sciences. The research made use of the Advanced Photon Source, a U.S. Department of Energy (DOE) Office of Science User Facility operated for the DOE Office of Science by Argonne National Laboratory under Contract No. DE-AC02-06CH11357.

REFERENCES

- (1) Bartlett, N. Xenon Hexafluoroplatinate(V) $Xe^{+}[PtF_{6}]^{-}$. *Proc. Chem. Soc.* **1962**, 218-&.
- (2) Drews, T.; Seppelt, K. The Xe₂+ ion Preparation and structure. *Angew. Chem.-Int. Edit. Engl.* **1997**, *36*, 273-274.
- (3) Drews, T.; Seidel, S.; Seppelt, K. Gold–Xenon Complexes. *Angew. Chem. Int. Ed.* **2002**, *41*, 454-456.
- (4) Britvin, S. N.; Kashtanov, S. A.; Krzhizhanovskaya, M. G.; Gurinov, A. A.; Glumov, O. V.; Strekopytov, S.; Kretser, Y. L.; Zaitsev, A. N.;

- Chukanov, N. V.; Krivovichev, S. V. Perovskites with the Framework-Forming Xenon. *Angew. Chem. Int. Ed.* **2015**, *54*, 14340-14344.
- (5) Britvin, S. N.; Kashtanov, S. A.; Krivovichev, S. V.; Chukanov, N. V. Xenon in Rigid Oxide Frameworks: Structure, Bonding and Explosive Properties of Layered Perovskite K₄Xe₃O₁₂. *J. Am. Chem. Soc.* **2016**, *138*, 13838-13841.
- (6) Zhu, L.; Liu, H. Y.; Pickard, C. J.; Zou, G. T.; Ma, Y. M. Reactions of Xenon with Iron and Nickel are Predicted in the Earth's Inner Core. *Nat. Chem.* **2014**, *6*, 644-648.
- (7) Stavrou, E.; Yao, Y. S.; Goncharov, A. F.; Lobanov, S. S.; Zaug, J. M.; Liu, H. Y.; Greenberg, E.; Prakapenka, V. B. Synthesis of Xenon and Iron-Nickel Intermetallic Compounds at Earth's Core Thermodynamic Conditions. *Phys. Rev. Lett.* **2018**, *120*, 6.
- (8) Yoo, C. S. Chemistry Under Extreme Conditions: Pressure Evolution of Chemical Bonding and Structure in Dense Solids. *Matter Radiat. Extremes* **2020**, *5*, 14.
- (9) Londono, D.; Kuhs, W. F.; Finney, J. L. Enclathration of Helium in Ice-II: The First Helium Hydrate. *Nature* **1988**, 332, 141-142.
- (10) Londono, D.; Finney, J. L.; Kuhs, W. F. Formation, Stability, and Structure of Helium Hydrate at High-Pressure. *J. Chem. Phys.* **1992**, *97*, 547-552.
- (11) Vos, W. L.; Finger, L. W.; Hemley, R. J.; Hu, J. Z.; Mao, H. K.; Schouten, J. A. A High-Pressure Van Der Waals Compound in Solid Nitrogen Helium Mixtures. *Nature* **1992**, *358*, 46-48.
- (12) Loubeyre, P.; Jeanlouis, M.; Letoullec, R.; Charongerard, L. High-Pressure Measurments of the He-Ne Binary Phase-Diagram at 296 K: Evidence for the Stability of a Stoichiometric Ne(He)₂ Solid. *Phys. Rev. Lett.* **1993**, 70, 178-181.
- (13) Sato, T.; Funamori, N.; Yagi, T. Helium Penetrates into Silica Glass and Reduces its Compressibility. *Nat. Commun.* **2011**, *2*, 5.
- (14) Shen, G.; Mei, Q.; Prakapenka, V. B.; Lazor, P.; Sinogeikin, S.; Meng, Y.; Park, C. Effect of Helium on Structure and Compression Behavior of SiO₂ Glass. *Proc. Natl. Acad. Sci.* **2011**, *108*, 6004-6007.
- (15) Sato, T.; Takada, H.; Yagi, T.; Gotou, H.; Okada, T.; Wakabayashi, D.; Funamori, N. Anomalous Behavior of Cristobalite in Helium under High Pressure. *Phys. Chem. Minerals* **2013**, *40*, 3-10.
- (16) Gunka, P. A.; Dziubek, K. F.; Gladysiak, A.; Dranka, M.; Piechota, J.; Hanfland, M.; Katrusiak, A.; Zachara, J. Compressed Arsenolite As₄O₆ and Its Helium Clathrate As₄O₆·2He. *Cryt. Growth Des.* **2015**, *15*, 3740-3745.
- (17) Sans, J. A.; Manjon, F. J.; Popescu, C.; Cuenca-Gotor, V. P.; Gomis, O.; Munoz, A.; Rodriguez-Hernandez, P.; Contreras-Garcia, J.; Pellicer-Porres, J.; Pereira, A. L. J.; Santamaria-Perez, D.; Segura, A. Ordered Helium Trapping and Bonding in Compressed Arsenolite: Synthesis of As₄O₆-2He. *Phys. Rev. B* **2016**, 93, 5.
- (18) Yagi, T.; Iida, E.; Hirai, H.; Miyajima, N.; Kikegawa, T.; Bunno, M. High-Pressure Behavior of a SiO₂ Clathrate Observed by using Various Pressure Media. *Phys. Rev. B* **2007**, *75*, *6*.
- (19) Dong, X.; Oganov, A. R.; Goncharov, A. F.; Stavrou, E.; Lobanov, S.; Saleh, G.; Qian, G.-R.; Zhu, Q.; Gatti, C.; Deringer, V. L.; Dronskowski, R.; Zhou, X.-F.; Prakapenka, V. B.; Konôpková, Z.; Popov, I. A.; Boldyrev, A. I.; Wang, H.-T. A Stable Compound of Helium and Sodium at High Pressure. *Nat Chem* **2017**, *9*, 440-445.
- (20) Miao, M. Helium Chemistry: React with Nobility. *Nat. Chem.* **2017**, *9*, 409-410.
- (21) Li, Y. W.; Feng, X. L.; Liu, H. Y.; Hao, J.; Redfern, S. A. T.; Lei, W. W.; Liu, D.; Ma, Y. M. Route to High- Energy Density Polymeric Nitrogen t-N via He-N Compounds. *Nat. Commun.* **2018**, *9*, 7.
- (22) Liu, Z.; Botana, J.; Hermann, A.; Valdez, S.; Zurek, E.; Yan, D.; Lin, H.-q.; Miao, M.-s. Reactivity of He with Ionic Compounds under High Pressure. *Nat. Commun.* **2018**, *9*, 951.

- (23) Gao, H.; Sun, J.; Pickard, C. J.; Needs, R. J. Prediction of Pressure-Induced Stabilization of Noble-Gas-Atom Compounds with Alkali Oxides and Alkali Sulfides. *Phys. Rev. Mater.* **2019**, *3*, 7.
- (24) Zhang, J.; Lv, J.; Li, H.; Feng, X.; Lu, C.; Redfern, S. A. T.; Liu, H.; Chen, C.; Ma, Y. Rare Helium-Bearing Compound FeO₂He Stabilized at Deep-Earth Conditions. *Phys. Rev. Lett.* **2018**, *121*, 255703.
- (25) Monserrat, B.; Martinez-Canales, M.; Needs, R. J.; Pickard, C. J. Helium-Iron Compounds at Terapascal Pressures. *Phys. Rev. Lett.* **2018**, *121*, 015301.
- (26) Bai, Y. H.; Liu, Z.; Botana, J.; Yan, D. D.; Lin, H. Q.; Sun, J.; Pickard, C. J.; Needs, R. J.; Miao, M. S. Electrostatic Force Driven Helium Insertion into Ammonia and Water Crystals Under Pressure. *Comm. Chem.* **2019**, 2, 7.
- (27) Liu, C.; Gao, H.; Wang, Y.; Needs, R. J.; Pickard, C. J.; Sun, J.; Wang, H. T.; Xing, D. Y. Multiple Superionic States in Helium-Water Compounds. *Nat. Phys.* **2019**, *15*, 1065-+.
- (28) Liu, C.; Gao, H.; Hermann, A.; Wang, Y.; Miao, M. S.; Pickard, C. J.; Needs, R. J.; Wang, H. T.; Xing, D. Y.; Sun, J. Plastic and Superionic Helium Ammonia Compounds under High Pressure and High Temperature. *Phys. Rev. X* **2020**, *10*, 11.
- (29) Hester, B. R.; dos Santos, A. M.; Molaison, J. J.; Hancock, J. C.; Wilkinson, A. P. Synthesis of Defect Perovskites $(He_{2-x} \square_x)(CaZr)F_6$ by Inserting Helium into the Negative Thermal Expansion Material CaZrF₆. *J. Am. Chem. Soc.* **2017**, *139*, 13284-13287.
- (30) Babel, D.; Tressaud, A.: Crystal Chemistry of Fluorides. In *Inorganic Solid Fluorides*; Hagenmuller, P., Ed.; Materials Science and Technology; Academic Press, Inc.: Orlando, 1985; pp 78-203.
- (31) Reinen, D.; Steffens, F. Structure and Bonding in Transition-Metal Fluorides $M^{II}Me^{IV}F_6$.A. Phase-Transitions. *Z. Anorg. Allg. Chem.* **1978**, 441, 63-82.
- (32) Greve, B. K.; Martin, K. L.; Lee, P. L.; Chupas, P. J.; Chapman, K. W.; Wilkinson, A. P. Pronounced Negative Thermal Expansion from a Simple Structure: Cubic ScF₃. *J. Am. Chem. Soc.* **2010**, *132*, 15496-15498.
- (33) Hancock, J. C.; Chapman, K. W.; Halder, G. J.; Morelock, C. R.; Kaplan, B. S.; Gallington, L. C.; Bongiorno, A.; Han, C.; Zhou, S.; Wilkinson, A. P. Large Negative Thermal Expansion and Anomalous Behavior on Compression in Cubic ReO₃-type A^{II}B^{IV}F₆: CaZrF₆ and CaHfF₆ *Chem. Mater.* **2015**, 27, 3912-3918.
- (34) Hester, B. R.; Hancock, J. C.; Lapidus, S. H.; Wilkinson, A. P. Composition, Response to Pressure, and Negative Thermal Expansion in $M^{11}B^{1V}F_6$ (M = Ca, Mg; B = Zr, Nb). *Chem. Mater.* **2017**, 29, 823-831.
- (35) Rivers, M.; Prakapenka, V. B.; Kubo, A.; Pullins, C.; Holl, C. M.; Jacobsen, S. D. The COMPRES/GSECARS Gas-Loading System for Diamond Anvil Cells at the Advanced Photon Source. *High Pressure Res.* **2008**, 28, 273-292.
- (36) Angel, R. J. The High-Pressure, High-Tempertaure Equation of State of Calcium Fluoride, CaF₂. *J. Phys. Condens. Matter* **1993**, *5*, L141-L144.
- (37) Boehler, R.; Kennedy, G. C. Equation of State of Sodium Chloride up to 32 kbar and 500°C. *J. Phys. Chem. Solids* **1980**, *41*, 517-523.
- (38) Touloukian, Y. S.; Kirby, R. K.; Taylor, R. E.; Lee, T. Y. R.: Thermal Expansion: Nonmetallic Solids. In *Thermophysical Properties of Matter*; Touloukian, Y. S., Ed.; Plenum: New York, 1970; Vol. 13; pp 1000.
- (39) Wang, K.; Reeber, R. R. Thermal Expansion of Alkali Halides at High Pressure: NaCl as an Example. *Phys. Chem. Minerals* **1996**, 23, 354-360.
- (40) Prescher, C.; Prakapenka, V. B. DIOPTAS: A Program for Reduction of Two-Dimensional X-ray Diffraction Data and Data Exploration. *High Pressure Res.* **2015**, 35, 223-230.
- (41) Larson, A. C.; Von Dreele, R. B.: GSAS General Structure Analysis System: Los Alamos Laboratory, 1987; Vol. Report LA-UR-86-748.
- (42) Toby, B. H. EXPGUI, a Graphical User Interface for GSAS. *J. Appl. Crystallogr.* **2001**, *34*, 210-213.

- (43) Toby, B. H.; Von Dreele, R. B. GSAS-II: The Genesis of a Modern Open-Source All Purpose Crystallography Software Package. *J. Appl. Crystallogr.* **2013**, *46*, 544-549.
- (44) Holtgrewe, N.; Greenberg, E.; Prescher, C.; Prakapenka, V. B.; Goncharov, A. F. Advanced integrated optical spectroscopy system for diamond anvil cell studies at GSECARS. *High Pressure Res.* **2019**, 39, 457-470.
- (45) Dove, M. T.; Fang, H. Negative Thermal Expansion and Associated Anomalous Physical Properties: Review of the Lattice Dynamics Theoretical Foundation. *Rep. Prog. Phys.* **2016**, *79*, 066503.
- (46) Fang, H.; Dove, M. T.; Phillips, A. E. Common Origin of Negative Thermal Expansion and other Exotic Properties in Ceramic and Hybrid Materials. *Phys. Rev. B* **2014**, *89*, 214103.
- (47) Sanson, A.; Giarola, M.; Mariotto, G.; Hu, L.; Chen, J.; Xing, X. R. Lattice Dynamics and Anharmonicity of CaZrF₆ from Raman

- Spectroscopy and Ab Initio Calculations. Mater. Chem. Phys. 2016, 180, 213-218
- (48) Mitchell, R. H.: *Perovskites: Modern and Ancient*; Almaz Press Inc.: Thunder Bay, Ontario, Canada, 2002.
- (49) Howard, C. J.; Kennedy, B. J.; Woodward, P. M. Ordered double perovskites a group-theoretical analysis. *Acta Crystallogr. Sect. B: Struct. Sci.* **2003**, *59*, 463-471.
- (50) Hester, B. R.; Wilkinson, A. P. Effects of Composition on Crystal Structure, Thermal Expansion, and Response to Pressure in ReO₃-type MNbF₆ (M= Mn and Zn). *J. Solid State Chem.* **2019**, 269, 428-433.
- (51) Hester, B. R.; Wilkinson, A. P. Negative Thermal Expansion, Response to Pressure and Phase Transitions in CaTiF₆. *Inorg. Chem.* **2018**, *57*, 11275-11281.

Insert Table of Contents artwork here

